Nanoscale

PAPER

View Article Online
View Journal | View Issue

Cite this: *Nanoscale*, 2017, **9**, 5299

High-performance thermoelectricity in edge-over-edge zinc-porphyrin molecular wires†

Mohammed Noori,‡[a,b] Hatef Sadeghi [a] and Colin J. Lambert *[a]

Received 12th December 2016,
Accepted 23rd March 2017

DOI: 10.1039/c6nr09598d

rsc.li/nanoscale

If high efficiency organic thermoelectric materials could be identified, then these would open the way to a range of energy harvesting technologies and Peltier coolers using flexible and transparent thin-film materials. We have compared the thermoelectric properties of three zinc porphyrin (ZnP) dimers and a ZnP monomer and found that the "edge-over-edge" dimer formed from stacked ZnP rings possesses a high electrical conductance, negligible phonon thermal conductance and a high Seebeck coefficient of the order of 300 μV K^{-1}. These combine to yield a predicted room-temperature figure of merit of $ZT \approx 4$, which is the highest room-temperature ZT ever reported for a single organic molecule. This high value of ZT is a consequence of the low phonon thermal conductance arising from the stacked nature of the porphyrin rings, which hinders phonon transport through the edge-over-edge molecule and enhances the Seebeck coefficient.

Introduction

Thermoelectric materials, which convert heat to electrical energy, could have an enormous impact on global energy consumption, but at present their efficiency is too low and the most efficient materials are toxic and have limited global supply. Recently, in an effort to overcome these limitations, thermoelectric effects in low-dimensional structures and molecular-scale systems have begun to be investigated.[1–14] Nanostructures are promising, because transport takes place through discrete energy levels and in molecular-scale junctions, this leads to room-temperature quantum interference, which opens further avenues for enhancing the conversion of heat into electrical energy.[15]

The efficiency of a thermoelectric (TE) material or device is determined by the dimensionless thermoelectric figure of merit $ZT = GS^2T/\kappa$, where G is the electrical conductance, T is temperature, S is the thermopower (Seebeck coefficient) and $\kappa = \kappa_{el} + \kappa_{ph}$ is the thermal conductance due to electrons (κ_{el}) and phonons (κ_{ph}). The Seebeck coefficient characterizes the ability of a thermoelectric material to convert heat to electricity and is defined as $S = -\Delta V/\Delta T$, where ΔV is the voltage difference generated between the two ends of the junction when a temperature difference ΔT is established between them.[7,16–19] Enhancing the efficiency of TE materials is not easy, because all parameters are correlated. For example at the fundamental level, the electronic properties G, S and κ_{el} are related, because they are all derived from the transmission coefficient $T_{el}(E)$ describing electrons of energy E passing from one electrode to other through a molecule (see Methods). In particular the Seebeck coefficient S is approximately proportional to the slope of $\ln T_{el}(E)$, evaluated at the Fermi energy E_F, whereas the electrical conductance is proportional to $T_{el}(E_F)$. Therefore, if the Fermi energy lies in a region of high slope, close to a transmission resonance then both G and S are enhanced.[20] On the other hand, to decrease the thermal conductance κ, which appears in the denominator of ZT, both electron and phonon transport must be engineered. Therefore, simultaneous consideration of both electron and phonon transport is needed to develop new materials for thermoelectricity.

Since only a few groups worldwide are able to measure the thermal conductance of single molecules, theoretical investigation is needed to identify new strategies to simultaneously suppress phonons and enhance S and G. Recent proposals to reduce phonon transport in molecular junctions include weakening the overlap between the continuum of vibrational states in the electrodes and discrete vibrational modes of the molecules,[21] taking advantage of the weak interaction between different parts of the molecules, as in π–π stacked structures[19] and using the low Debye frequency of electrodes to filter high-frequency phonons.[20] The challenge is to identify new materials and device structures in which such strategies can be

[a]*Quantum Technology Centre, Department of Physics, Lancaster University, Lancaster LA1 4YB, UK. E-mail: h.sadeghi@lancaster.ac.uk, c.lambert@lancaster.ac.uk*
[b]*Department of Physics, College of Science, Thi-Qar University, Thi-Qar, Iraq*
†Electronic supplementary information (ESI) available. See DOI: 10.1039/c6nr09598d
‡These authors contributed equally to this work.

realized in the laboratory. In this paper, we present a comparative theoretical study of the thermoelectric properties of four different zinc porphyrin structures and elucidate a new strategy for simultaneously increasing their thermopower and reducing their thermal conductance leading to a high value of ZT.

Methods

The geometry of each structure consisting of gold electrodes and a single zinc porphyrin molecule was relaxed to a force tolerance of 20 meV Å^{-1} using the SIESTA[28] implementation of density functional theory (DFT), with a double-ζ polarized basis set (DZP) and generalized gradient functional approximation (GGA-PBE) for the exchange and correlation functionals,[30,31] which is applicable to arbitrary geometries. A real-space grid was defined with an equivalent energy cutoff of 150 Ry. From the relaxed xyz coordinate of the system, sets of xyz coordinates were generated by displacing each atom in positive and negative x, y, and z directions by $\delta q' = 0.01$ Å. The forces in three directions $q_i = (x_i, y_i, z_i)$ on each atom were then calculated by DFT without geometry relaxation. These values of force are combined with the method described in ref. 20 to calculate the dynamical matrix and thermal conductance due to phonons.

To calculate the electronic properties of the molecules in the junction, from the converged DFT calculation, the underlying mean-field Hamiltonian H was combined with our quantum transport code, GOLLUM[29] to calculate the transmission coefficient $T_{el}(E)$ for electrons of energy E passing from the source to the drain. The electrical conductance $G_{el}(T) = G_0 L_0$, the electronic contribution of the thermal conductance $\kappa_{el}(T) = (L_0 L_2 - L_1^2)/hTL_0$ = and the thermopower $S(T) = -L_1/eTL_0$ of the junction are calculated from the electron transmission coefficient $T_{el}(E)$ where $L_n(T) = \int_{-\infty}^{\infty} dE(E - E_F)^n T_{el}(E)\left(-\frac{\partial f(E,T)}{\partial E}\right)$ and $f(E,T)$ is the Fermi–Dirac probability distribution function $f(E,T) = (e^{(E-E_F)/K_BT} + 1)^{-1}$, T is the temperature, E_F is the Fermi energy, $G_0 = 2e^2/h$ is the conductance quantum, e is electron charge, and h is the Planck's constant.

Results and discussion

Fig. 1 shows four different zinc porphyrin (ZnP) structures investigated below. The first **1** is a ZnP monomer.[22] Structure **2** is an edge-over-edge ZnP dimer, in which two ZnPs are locked together by *meso*-position pyridines.[23,24] Structure **3** comprises two ZnPs connected by an oligoyne linker,[22,25,26] while **4** comprises two ZnPs connected through *meso*-position pyridines.[27] In what follows, our aim is to demonstrate that of the above structures, the edge-over-edge ZnP dimer **2** is by far the most efficient thermoelectric energy converter. From a structural point of view, this arises because the pyridyl rings of **2** are locked and therefore ring rotation, which would otherwise

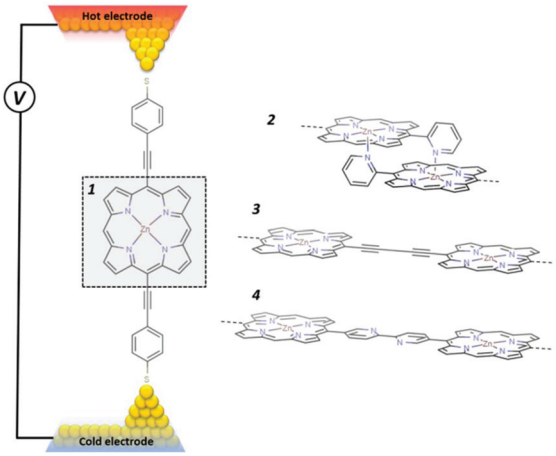

Fig. 1 The device structures investigated consist of four different zinc porphyrin (ZnP) monomer structures. (**1**) Edge-over-edge ZnP, (**2**) a ZnP-dimer linked by an oligoyne chain, (**3**) a ZnP-dimer linked by two pyridyl rings (**4**).

reduce the electrical conductance, is eliminated. Secondly, the edge-over-edge rigid conformation of **2** increases its rigidity, which pushes the internal vibrational modes to higher frequencies. This reduces room temperature thermal conductance, because modes with frequencies greater than ~25 meV do not contribute significantly. Thirdly, longitudinal modes entering one end of the edge-over-edge molecule must convert to flexural modes to pass from one porphyrin to the other, which creates extra phonon scattering and reduces thermal conductance.

For the structures of Fig. 1, Fig. 2 show the transmission coefficients for electrons with energy E and phonons of energy $\hbar\omega$, passing through a molecule from the left electrode to the right electrode, calculated using the method described in ref. 20. We first carry out geometrical optimization of each molecule placed between two gold electrodes using the SIESTA[28] implementation of density functional theory (DFT) to find the ground state optimized positions of the atoms relative to each other (see Methods). From the ground state geometry, we obtain the mean-field Hamiltonian of each system comprising both electrodes and molecules and use our transport code GOLLUM[29] to calculate the transmission coefficients $T_{el}(E)$ (see Methods). In each case the optimal angle between the porphyrins is zero, which corresponds to the maximum conductance that could be obtained.[22] The electronic transport properties of **1** and **3** have been studied experimentally in the literature,[22] so we used these to benchmark our calculations. As shown in Table S1 of the ESI,† our calculated conductances for these molecules are in good agreement with experiment. The electron transmission of **4** is much smaller than **1**, **2** and **3**, whereas the transmission of **2** is either equal to that of **3** near the HOMO resonance or lower in the vicinity of the middle of the HOMO–LUMO gap. As shown in Fig. (SI2†), this is reflected in the electrical conductance as a function of temperature.

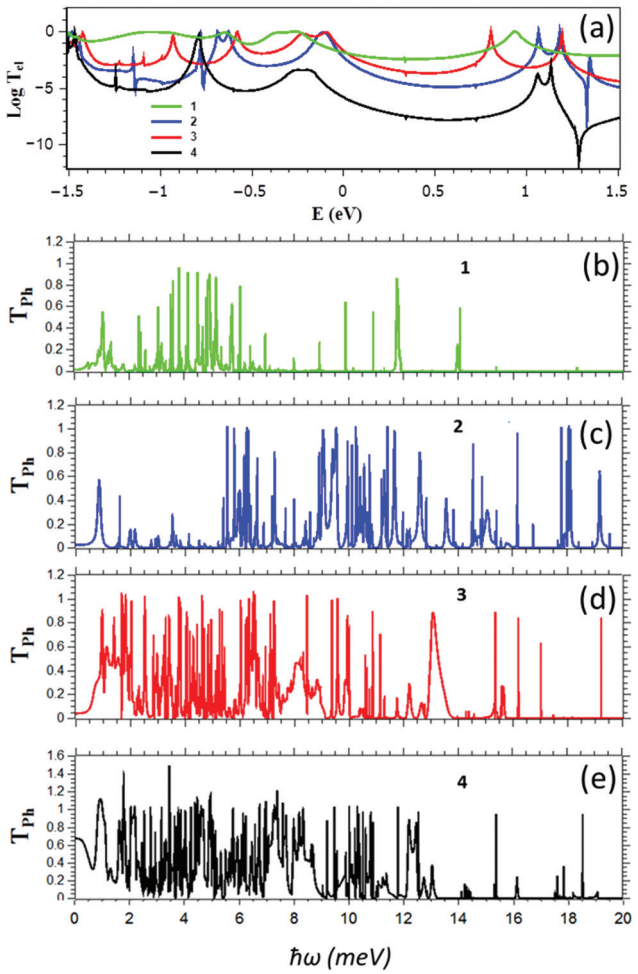

Fig. 2 (a) Electron transmission coefficients as a function of energy and (b–e) phonon transmission coefficients as a function of $\hbar\omega$ for the ZnP monomer **1**, the edge-over-edge ZnP **2**, the ZnP dimer connected *via* an oligoyne chain **3** and ZnP dimer connected through pyridyl rings **4**.

To calculate the vibrational properties of each structure, we use the harmonic approximation to construct the dynamical matrix D. Each atom is displaced from its ground-state equilibrium position by $\delta q'$ and $-\delta q'$ in the x, y, and z directions and the forces on all atoms calculated in each case. For $3n$ degrees of freedom (n = number of atoms), the $3n \times 3n$ dynamical matrix $D_{ij} = (F_i^q(\delta q'_j) - F_j^q(-\delta q'_j))/2M_{ij}\delta q'_j$ is constructed, where F and M are the force and mass matrices (see ref. 20 for more details). For an isolated molecule, the square root of the given values of D determines the frequencies ω associated with the vibrational modes of the molecule in the junction (see the ESI†). For a molecule within a junction, the dynamical matrix describes an open system composed of the molecule and two semi-infinite electrodes and is used to calculate the transmission coefficient $T_{ph}(\omega)$ for phonons with energy $\hbar\omega$ passing through the molecule from the right to the left electrodes.[20]

Fig. 2b–e shows $T_{ph}(\omega)$ for the four structures of Fig. 1. It is apparent that the widths of the resonances in the edge-over-edge ZnP-dimer **2** are smaller than those of the other structures and the low energy phonons (in the range 2–5 meV) are either suppressed or pushed to higher frequencies. This can be demonstrated using the participation ratio of the dimer molecular cores **2**, **3** and **4** and comparing the integrated density of states $N(\hbar\omega)$ of **2**, **3** and **4**. As shown in Fig. S1 of the ESI,† the participation ratio of the molecule core (ZnPs and linkers) connected to the gold surface is mostly due to the in-plane (PRy) and out of plane (PRx) transverse modes in structures **3** and **4**, whereas out-of plane transverse modes are mainly suppressed or converted to in-plane transverse modes and moved to the higher frequency, reflecting the higher rigidity of the edge-over-edge structure. In addition, the integrated density of states is almost the same for **3** and **4**, whereas for low frequencies, the integrated density of states of **2** is smaller than **3** and **4**. This means the thermal conductance is reduced significantly in **2**, because transmission of the low energy modes is suppressed due to the scattering from in-plane modes to cross-plane transverse modes. In addition, some modes are pushed to higher frequency, although this is smaller effect compared with the suppression of low frequency transmission. Overall, these two effects combine to yield a lower phonon thermal conductance in **2**.

The thermal conductance of the junction ($\kappa = \kappa_{ph} + \kappa_{el}$) is obtained by summing the contributions from both electrons (κ_{el}) and phonons (κ_{ph}). The electronic (phonon) thermal conductances are calculated from the electron (phonon) transmission coefficients shown in Fig. 2a–e. Fig. 3a shows that the ZnP monomer **1** has the lowest value of κ_{ph} while **4** has the highest. This is counter-intuitive, because one would expect a higher thermal conductance for shorter molecules. However, due to the more rigid nature of the monomer, its vibrational modes are pushed to higher frequencies and therefore their contribution to the room temperature conductance is suppressed. In addition, Fig. 3b and c show that the thermal conductance due to the electrons κ_{el} of the dimer ZnP **3** is higher than those of the edge-over-edge ZnP and structures **1** and **4** for a wide range of energy in the vicinity of DFT predicted Fermi energy. The crucial point is that almost for all Fermi energies, the electronic contribution to the thermal conductance is higher than the phonon contribution. This is significant, because to achieve a high-ZT material, one needs to only focus on engineering the electronic properties of structure **2**.

To examine the thermoelectric properties of **1–4**, we obtained the Seebeck coefficient of all structures from the electron transmission coefficient $T_{el}(E)$, as described in the Methods. Fig. 4a shows the Seebeck coefficients as a function of Fermi energy E_F (and also as a function of temperature in Fig. S3 of the ESI†) and reveals that the edge-over-edge ZnP dimer **2** has a higher Seebeck coefficient than **1**, **3** and **4** due to the higher slope of $\ln T_{el}(E_F)$ over a wide range of Fermi energies between the HOMO and LUMO. Since the electronic contribution to the thermal conductance is higher in **1**, **2** and **3**, the contribution of the phonons is negligible. Furthermore the electrical conductance is proportional to the electronic thermal conductance, so they cancel each other in ZT. Consequently as shown in Fig. 4b, due to the high Seebeck

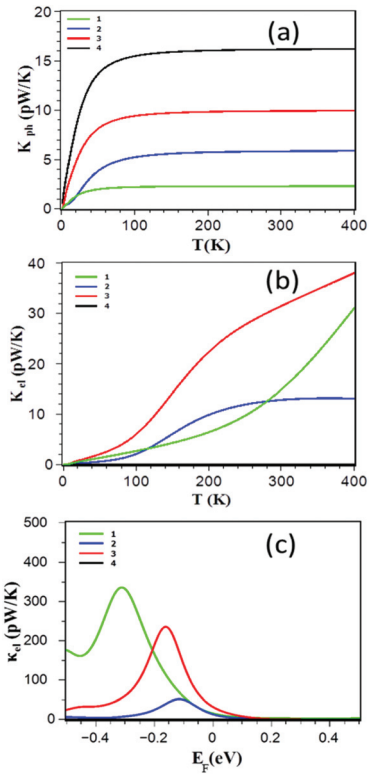

Fig. 3 (a) Phonon thermal conductances (b) electronic thermal conductance as a function of temperature, (c) room-temperature electronic thermal conductance as a function of Fermi energy E_F calculated using the DFT-predicted Fermi energy. The results are shown for the ZnP monomer **1**, the edge-over-edge ZnP **2**, the ZnP dimer connected through an oligoyne chain **3** and the ZnP-dimer connected through pyridyl rings **4**.

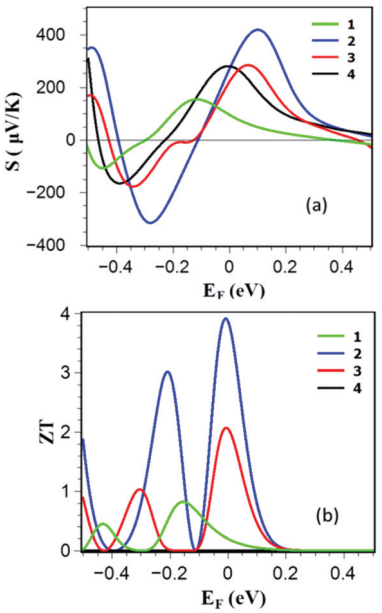

Fig. 4 (a) Seebeck coefficient S and (b) full thermoelectric figure of merit ZT as a function of Fermi energy for the ZnP monomer **1**, edge-over-edge ZnP **2**, ZnP connected through an oligoyne chain **3** and ZnP-dimer connected through pyridyl rings **4**.

coefficient of the edge-over-edge dimer, a ZT as high as ≈4 is obtained when E_F lies in a wide energy window in the vicinity of the DFT-predicted Fermi energy. Fig. 4b also shows that the less-rigid structure **4** is not promising for efficient conversion of the heat to electricity. Although all of these structures are made from ZnP, this study shows the importance of the molecular design. The more rigid edge-over-edge ZnP dimer **2** shows a very high ZT, whereas the less conductive structure **3** is unattractive for thermoelectricity.

To our knowledge, there currently exist no measurements of the Seebeck coefficient of porphyrins and no measurements of their ZT. The Seebeck coefficient of n-alkanedithiol (ADT) (n = 2, 3, 4, 5, 6, 8) was found to range from 6.8 to 2.4 μV K^{-1}, depending on the length n,[32,33] whereas 1,4-benzenedithiol (BDT), 4,4′-dibenzenedithiol (DBDT) and 4,4″-tribenzenedithiol (TBDT) attached to Au electrodes have been measured by several groups[34–41] and found to increase with the number of phenyl rings, ranging from 7 μV K^{-1} to 16 μV K^{-1}, by changing the terminal groups, measurements on 1,4-bis((trimethylstannyl)methyl)-n-phenyl (n = 1, 2, 3, 4) revealed that the Seebeck coefficient increased to 24 μV K^{-1} for the longest molecules. On the other hand 1,4-n-phenylenediamine (PDA) (n = 1, 2, 3) was found to have lower values in the range of 2.1–10.4 μV K^{-1}.[32,42,43] These values are comparable to the Seebeck coefficient of oligothiophenes, which can be as high as 14.8 μV K^{-1} for ethanethioate-terminated terthiophenes on gold.[44]

Changing the terminal groups to pyridine generally switches transport towards the LUMO and changes the sign of the Seebeck coefficient. For example the Seebeck coefficients of 4,4′-bipyridine and 1,2-di(4-pyridyl)ethylene attached to gold electrodes were found to be approximately −9 μV K^{-1} and −10 μV K^{-1} respectively.[43,45]

Fullerenes tend to have higher Seebeck coefficients, ranging from −10 to −30 μV K^{-1} for C_{60} with different metallic electrodes[46] to −33 μV K^{-1} for C_{60} dimers[47] and up to −31.6 μV K^{-1} C_{82} endohedral fullerenes.[48] The sign of the endohedral fullerene $Sc_3N@C_{80}$ was shown to be sensitive to pressure, ranging from −25 μV K^{-1} to +25 μV K^{-1}, depending on the orientation of the molecule on a gold substrate.[49]

The length dependent thermal conductance in Au-alkanethiol-SiO_2 junctions by the scanning thermal microscopy (SThM) technique has been measured to vary from 25 pW K^{-1} for the shortest chains to 10 pW K^{-1} for chains of 18 carbon atoms.[50] The thermal conductance of Au-alkanedithol (n = 8, 9, 10)-GaAs junctions at room temperature[51] was measured to be approximately 27 MW m^{-2} K^{-1}, assuming a 1 nm^2 footprint per molecule, this equates to 27 pW K^{-1} per molecule. Values ranging from 35 to 65 MW m^{-2} K^{-1} were measured for different terminal groups.[52]

Single-molecule thermoelectricity is a rapidly expanding field of fundamental research and our paper is aimed primarily at further developing our understanding at the single-mole-

cule level. Acquisition of the fundamental understanding of single-molecule thermoelectricity will underpin the design and synthesis of high-performance molecular films, but will not be sufficient, because a range of additional issues arise when single molecules are placed in parallel to form a molecular film. Ref. 53 discusses the question of how a statistical ensemble of single-molecule conductances and Seebeck coefficients combine in parallel to yield the thermoelectric properties of a dilute molecular film and concludes that a conductance-weighted single-molecule Seebeck coefficient is the relevant quantity. For more dense films, thermoelectric properties may be modified by intermolecular interactions, although as mentioned above, measurements of single-molecule thermal conductances of alkanes[50] are comparable to the thermal conductance per molecule obtained from the measurements on molecular films[51,52] and therefore at least for alkanes, such interactions do not appear to be significant.

Conclusions

In summary, we have compared the thermoelectric properties of three ZnP dimers and a ZnP monomer and found that the edge-over-edge-like dimer possesses a negligible phonon thermal conductance and a high Seebeck coefficient of the order of 300 μV K^{-1}. These transport properties combine to yield a room-temperature figure of merit of $ZT \approx 4$, which is the highest room-temperature ZT ever reported for an organic material. This high ZT value is a consequence of low phonon thermal conductance, which arises from the edge-over-edge stacking of the porphyrin rings and hinders phonon transport through the molecule.

Acknowledgements

This work is supported by UK EPSRC grants EP N017188/1, EP/M014452/1, the European Union Marie-Curie Network MOLESCO 606728 and the Ministry of Higher Education and Scientific Research, Thi-Qar University, Iraq. We dedicate this paper to the memory of the late Thomas Wandlowski, a world-leading scientist and a true friend, whose premature passing is a great loss to the molecular-electronics community.

References

1 H. Sadeghi, S. Sangtarash and C. J. Lambert, *Sci. Rep.*, 2015, **5**, 9514–9520.
2 M. Christensen, A. B. Abrahamsen, N. B. Christensen, F. Juranyi, N. H. Andersen, K. Lefmann, J. Andreasson, C. R. Bahl and B. B. Iversen, *Nat. Mater.*, 2008, **7**, 811–815.
3 G. Joshi, H. Lee, Y. Lan, X. Wang, G. Zhu, D. Wang, R. W. Gould, D. C. Cuff, M. Y. Tang and M. S. Dresselhaus, *Nano Lett.*, 2008, **8**, 4670–4674.
4 W. Kim, S. L. Singer, A. Majumdar, D. Vashaee, Z. Bian, A. Shakouri, G. Zeng, J. E. Bowers, J. M. Zide and A. C. Gossard, *Appl. Phys. Lett.*, 2006, **88**, 242107.
5 R. Venkatasubramanian, E. Siivola, T. Colpitts and B. O'quinn, *Nature*, 2001, **413**, 597–602.
6 L. Hicks, T. Harman, X. Sun and M. Dresselhaus, *Phys. Rev. B: Condens. Matter*, 1996, **53**, R10493.
7 P. Reddy, S.-Y. Jang, R. A. Segalman and A. Majumdar, *Science*, 2007, **315**, 1568–1571.
8 A. I. Hochbaum, R. Chen, R. D. Delgado, W. Liang, E. C. Garnett, M. Najarian, A. Majumdar and P. Yang, *Nature*, 2008, **451**, 163–167.
9 K. Baheti, J. A. Malen, P. Doak, P. Reddy, S.-Y. Jang, T. D. Tilley, A. Majumdar and R. A. Segalman, *Nano Lett.*, 2008, **8**, 715–719.
10 A. I. Boukai, Y. Bunimovich, J. Tahir-Kheli, J.-K. Yu, W. A. Goddard Iii and J. R. Heath, *Nature*, 2008, **451**, 168–171.
11 K. Schwab, E. Henriksen, J. Worlock and M. L. Roukes, *Nature*, 2000, **404**, 974–977.
12 K. Uchida, S. Takahashi, K. Harii, J. Ieda, W. Koshibae, K. Ando, S. Maekawa and E. Saitoh, *Nature*, 2008, **455**, 778–781.
13 X. Zheng, W. Zheng, Y. Wei, Z. Zeng and J. Wang, *J. Chem. Phys.*, 2004, **121**, 8537–8541.
14 M. Paulsson and S. Datta, *Phys. Rev. B: Condens. Matter*, 2003, **67**, 241403.
15 L. A. Algharagholy, Q. Al-Galiby, H. A. Marhoon, H. Sadeghi, H. M. Abduljalil and C. J. Lambert, *Nanotechnology*, 2015, **26**, 475401.
16 M. Wierzbicki and R. Świrkowicz, *J. Phys.: Condens. Matter*, 2010, **22**, 185302.
17 C. S. Lau, H. Sadeghi, G. Rogers, S. Sangtarash, P. Dallas, K. Porfyrakis, J. Warner, C. J. Lambert, G. A. D. Briggs and J. A. Mol, *Nano Lett.*, 2015, **16**, 170–176.
18 N. A. Zimbovskaya, *J. Phys.: Condens. Matter*, 2014, **26**, 275303.
19 H. Sadeghi, S. Sangtarash and C. J. Lambert, *Beilstein J. Nanotechnol.*, 2015, **6**, 1176–1182.
20 H. Sadeghi, S. Sangtarash and C. J. Lambert, *Nano Lett.*, 2015, **15**, 7467–7472.
21 R. Y. Wang, R. A. Segalman and A. Majumdar, *Appl. Phys. Lett.*, 2006, **89**, 173113.
22 G. Sedghi, V. M. García-Suárez, L. J. Esdaile, H. L. Anderson, C. J. Lambert, S. Martín, D. Bethell, S. J. Higgins, M. Elliott and N. Bennett, *Nat. Nanotechnol.*, 2011, **6**, 517–523.
23 R. T. Stibrany, J. Vasudevan, S. Knapp, J. A. Potenza, T. Emge and H. J. Schugar, *J. Am. Chem. Soc.*, 1996, **118**, 3980–3981.
24 J. Vasudevan, R. T. Stibrany, J. Bumby, S. Knapp, J. A. Potenza, T. J. Emge and H. J. Schugar, *J. Am. Chem. Soc.*, 1996, **118**, 11676–11677.
25 A. K. Burrell, D. L. Officer, P. G. Plieger and D. C. Reid, *Chem. Rev.*, 2001, **101**, 2751–2796.
26 I. Beletskaya, V. S. Tyurin, A. Y. Tsivadze, R. Guilard and C. Stern, *Chem. Rev.*, 2009, **109**, 1659–1713.

27 K. F. Cheng, C. M. Drain and K. Grohmann, *Inorg. Chem.*, 2003, **42**, 2075–2083.
28 J. M. Soler, E. Artacho, J. D. Gale, A. García, J. Junquera, P. Ordejón and D. Sánchez-Portal, *J. Phys.: Condens. Matter*, 2002, **14**, 2745.
29 J. Ferrer, C. J. Lambert, V. M. García-Suárez, D. Z. Manrique, D. Visontai, L. Oroszlany, R. Rodríguez-Ferradás, I. Grace, S. Bailey and K. Gillemot, *New J. Phys.*, 2014, **16**, 093029.
30 J. P. Perdew, K. Burke and M. Ernzerhof, *Phys. Rev. Lett.*, 1996, **77**, 3865.
31 B. Hammer, L. B. Hansen and J. K. Nørskov, *Phys. Rev. B: Condens. Matter*, 1999, **59**, 7413.
32 J. A. Malen, *et al.*, *Nano Lett.*, 2009, **9**, 1164.
33 S. Y. Guo, G. Zhou and N. J. Tao, *Nano Lett.*, 2013, **13**, 4326.
34 A. Tan, S. Sadat and P. Reddy, *Appl. Phys. Lett.*, 2010, **96**, 013110.
35 A. Tan, *et al.*, *J. Am. Chem. Soc.*, 2011, **133**, 8838.
36 S. K. Lee, *et al.*, *Nano Lett.*, 2014, **14**, 5276.
37 Y. Kim, *et al.*, *Appl. Phys. Lett.*, 2016, **109**, 033102.
38 D. Z. Manrique, Q. Al-Galiby, W. Hong and C. J. Lambert, *Nano Lett.*, 2016, **16**, 1308–1316.
39 M. Tsutsui, M. Taniguchi and T. Kawai, *Nano Lett.*, 2008, **8**, 3293.
40 T. Morikawa, *et al.*, *Nanoscale*, 2014, **6**, 8235.
41 S. Kaneko, *et al.*, *Appl. Phys. Express*, 2015, **8**, 095503.
42 D. Kim, P. S. Yoo and T. Kim, *J. Korean Phys. Soc.*, 2015, **66**, 602.
43 T. Kim, *et al.*, *Nano Lett.*, 2014, **14**, 794.
44 W. B. Chang, *et al.*, *Chem. Mater.*, 2014, **26**, 7229.
45 J. R. Widawsky, *et al.*, *Nano Lett.*, 2012, **12**, 354.
46 S. K. Yee, *et al.*, *Nano Lett.*, 2011, **11**, 4089.
47 C. Evangeli, *et al.*, *Nano Lett.*, 2013, **13**, 2141.
48 S. K. Lee, *et al.*, *Nanoscale*, 2015, **7**, 20497.
49 L. Rincon-Garcia, *et al.*, *Nat. Mater.*, 2016, **15**, 289.
50 T. Meier, *et al.*, *Phys. Rev. Lett.*, 2014, **113**, 060801.
51 R. Y. Wang, R. A. Segalman and A. Majumdar, *Appl. Phys. Lett.*, 2006, **89**, 173113.
52 M. D. Losego, *et al.*, *Nat. Mater.*, 2012, **11**, 502.
53 C. J. Lambert, H. Sadeghi and Q. Al-Galiby, *C. R. Phys.*, 2016, **17**(10), 1084.